JOURNAL OF MATERIALS SCIENCE **35** (2000) 2625–2633

Structure and properties of rapidly solidified Al-Zr-Ti alloys

P. MÁLEK, M. JANEČEK, B. SMOLA
Department of Metal Physics, Charles University, Ke Karlovu 5, 12116 Prague 2, Czech Republic

P. BARTUŠKA
Institute of Physics, Academy of Sciences of Czech Republic, Na Slovance 2, 18040 Prague 8, Czech Republic

J. PLEŠTIL
Institute of Macromolecular Chemistry, Academy of Sciences of Czech Republic, Heyrovského nám. 1, 16000 Prague 6, Czech Republic
E-mail: malek@apollo.karlov.mff.cuni.cz

The Al-Zr-Ti system has recently been suggested as a candidate for Al-based materials capable of retaining a high strength during a long term exposure to high temperatures up to 700 K. The Al-1.25 at.% (Zr+Ti) alloys with a variable Zr : Ti ratio were rapidly solidified using the melt spinning method. The solidification structure was found inhomogeneous along the direction perpendicular to the ribbon plane and dependent on the Zr : Ti ratio. The microhardness values were correlated with the structure and chemical composition. The presence of second phase particles in the as melt-spun ribbons was proved by SAXS experiments. X-ray and electron diffraction experiments enabled to identify most of particles as the metastable $Al_3(Zr_xTi_{1-x})$ phase with the cubic $L1_2$ structure. Especially in the Zr-rich alloys, these particles precipitated preferentially in a fan-shaped morphology. The grains of the Ti-rich alloys were nearly free of these particles.

1. Introduction

A substitution of high-strength Al-based alloys for Ti-based ones in elevated temperature applications (up to 700 K) is a challenging task of modern metallurgy. One of the ways how to solve this task is to design Al-based alloys with a high volume fraction of very small second phase particles which are stable at elevated temperatures and contribute to the high strength through a dispersion or precipitation strengthening. Current age-hardenable aluminium alloys cannot be used for this purpose as any annealing at temperatures above about 423 K results in a coarsening or dissolution of strengthening phases and, therefore, in a drop of strength. New compositions and producing methods must be sought.

The suitable additives for elevated temperature Al-based alloys have to meet the following requirements:

– a capability to form intermetallic phases with Al which have a similar structure to Al-matrix,

– a low equilibrium solid solubility up to temperatures of 700 K in order to avoid the dissolution of strengthening phases,

– a low diffusivity in Al in order to slow down the diffusion controlled coarsening of particles of strengthening phases.

Transition metals as Fe, Ni, Cr, Ti, V or Zr meet these requirements [1]. Zirconium has a special position among these additives. It forms the Al_3Zr intermetallic phase the tetragonal DO_{23} structure of which has a low lattice mismatch to Al-matrix (about 2.9% [2]). The formation of this equilibrium phase is usually preceded by the formation of a metastable Al_3Zr phase the cubic $L1_2$ structure of which has even smaller lattice mismatch (about 0.7% [3]). The equilibrium solid solubility of Zr in Al is very small and reaches its maximum of 0.28 wt.% at 934 K [4]. The diffusion rate of Zr in Al is the lowest among the additives mentioned above [5]. For these reasons, zirconium seems to be one of the most suitable additives for designing the Al-based alloys for elevated temperature applications.

Conventional ingot metallurgy processing route results in massive segregations and formation of coarse primary particles and the desired structure with a homogeneous distribution of small second phase particles cannot be formed. On the other hand, rapid solidification techniques with quenching rates up to 10^6 Ks^{-1} enable to extend the solid solubility limits, suppress the formation of primary particles and homogenize and refine the solidified structure [6]. All these effects are favourable for the designing of Al-alloys for elevated

temperature applications. In the rapidly solidified binary Al-Zr alloys, the solid solubility limit can be extended up to 4.9 wt.% [1] and the desirable distribution of second phase particles contributing to a high strength can be formed through a decomposition of the supersaturated matrix during a subsequent annealing.

The strengthening effect of second phase particles generally decreases with increase in their size. In order to retain a high strength at elevated temperatures, the particle coarsening has to be avoided. According to the theory of diffusion controlled ripening [7, 8] the coarsening rate decreases among others with decreasing interfacial energy, i.e. with decreasing lattice mismatch between the strengthening phase and matrix. The metastable Al_3Zr phase should be, therefore, more resistant to coarsening and contribute more to the high strength at high temperatures than the equilibrium one. Lattice mismatches of both modifications of the Al_3Zr phase may be further reduced by ternary additives as V, Hf or Ti [9, 10] which would result in a better structure and strength stability. An extensive study on the Al-Zr-V system confirmed this expectation. Unfortunately, the formation of an additional $Al_{10}V$ phase especially at grain boundaries of the Al-matrix deteriorated the mechanical properties [11, 12]. The selection of Ti as the ternary additive should avoid this difficulty. The measurement of the coarsening rate in the Al-Zr-Ti alloy containing about 1 vol.% of the $Al_3(Zr_{0.75}\ Ti_{0.25})$ phase revealed an extraordinary stability of this alloy at 698 K [13]. The Al-Zr-Ti system with a higher Zr and Ti content was, therefore, chosen for our experiments.

The main objective of our investigation was to study the structure of the as melt-spun ribbons of Al-Zr-Ti alloys with varying Zr : Ti ratio. In order to obtain a complex information a variety of experimental methods was used. A special attention was paid to the structure and composition inhomogeneities, to the phase composition and to their influence on microhardness.

2. Material and procedure

The Al-Zr-Ti alloys with the equilibrium phase composition of Al-5 vol.% $Al_3(Zr_xTi_{1-x})$ in a precipitated state were used in our experiments. The stoichiometric parameters $x = 1$, 0.75, 0.5, 0.25 and 0 were chosen. The nominal chemical compositions of these alloys are given in Table I. The precastings prepared from 99.995% Al, Al-6 wt.% Zr and Al-10 wt.% Ti master alloys were remelted by the induction melting in a boron-nitride crucible and the melt was then ejected using argon gas pressure (5×10^4 Pa) onto a rotating copper wheel located in a chamber evacuated to 5×10^{-3} Pa. The melt spun ribbons of the thickness between 15 and 40 μm and the width between 1 and 2 mm were prepared.

The chemical composition was studied using the X-ray microanalyser JEOL Superprobe 733. The energy dispersive (EDX) analyses were performed both on the as received chilled and free surfaces, whereas metallographically processed transversal sections were analyzed by the wave length analysis (WDA) technique. In order to control the homogeneity and possible directionality of the chemical composition the point analyses were carried out at different places along the longitudinal and transversal directions of ribbons.

The solidification structure was studied on the transversal and longitudinal sections using light (OM) and scanning electron (SEM) microscopy. The specimens for light microscopy investigation were mounted into special holders, fixed in DEMOTEC, polished mechanically and electrolytically in the solution of 20% $HClO_4$ in ethanol at 253 K and 30 V, and etched chemically in the Dix-Keller etching solution. The specimens for scanning electron microscopy investigation were covered electrolytically by pure Ni, mounted and polished mechanically or electrolytically (20% $HClO_4$, 80% ethanol at 243 K and 15 V).

The Knoop microhardness was measured at room temperature on the metallographically polished longitudinal sections using a LECO M-400-A microhardness tester at the load of 10 g and dwell time of 15 s. Some specimens were slightly etched prior to microhardness measurements to allow the correlation of the microhardness value with the structure.

The small angle X-ray scattering (SAXS) investigation of the ribbons was performed using a Kratky camera equipped with a linear position sensitive detector. The measured scattering intensity was converted into the normalized intensity by means of a Lupolen standard.

The phase composition was studied using the X-ray diffraction analysis. The measurement was performed using Cu-K_α radiation in the diffractometer Siemens-Kristalloflex at room temperature with the scanning regime 0.02°/30 s. The Si reference powder was added to some samples as an X-ray peak position standard.

The internal structure was studied using the transmission electron microscopy (TEM). The ribbons were thinned electrolytically in the 66% HNO_3-33% CH_3OH

TABLE I Chemical composition of the Al-$Al_3(Zr_xTi_{1-x})$ alloys in wt.%

	Nominal composition		EDX analysis chilled surface		EDX analysis free surface	
x	Zr	Ti	Zr	Ti	Zr	Ti
1	4.1	—	4.0 ± 0.2	—	3.9 ± 0.5	—
0.75	3.1	0.55	3.1 ± 0.2	0.6 ± 0.1	3.1 ± 0.6	0.6 ± 0.1
0.5	2.1	1.1	2.1 ± 0.2	1.2 ± 0.1	2.3 ± 0.4	1.4 ± 0.1
0.25	1.0	1.65	1.0 ± 0.1	1.7 ± 0.1	0.9 ± 0.3	1.8 ± 0.1
0	—	2.2	—	2.3 ± 0.1	—	2.4 ± 0.2

solution. The observations were carried out in an analytical electron microscope JEOL 2000 FX at 200 kV.

3. Experimental results

3.1. Solidification structure and microhardness

The rates of solidification and cooling of the solidified material decrease with increasing distance from the contact (chilled) surface in the melt spinning process. This gradient may significantly influence the structure and physical properties and, therefore, both surfaces of the ribbons have to be investigated separately.

No particles were observed at the chilled surface except for the Al-Ti alloy where relatively coarse (up to 10 μm) oval particles were observed. The presence of Fe was found out in the spectrum taken from these particles. The results of the EDX analysis (Table I) correspond well with the nominal composition and show no significant directionality in the surface plane.

Numerous light particles inhomogeneously distributed within the structure were observed at the free surface of all materials. Their size was usually between 1 and 5 μm and a slight peak of oxygen was found in their spectrum. A fine grained structure with equiaxed grains of the size about 1 μm was observed in regions containing less particles (Fig. 1). The results of the EDX analysis given in Table I reveal a broader scatter especially in the content of Zr at the free surface. However, both the content of Zr and Ti correspond to the nominal compositions within the experimental error of the method used (about 0.2 wt.%) and the chemical composition seems to be reasonably homogeneous.

The solidification structure is not homogeneous along the direction perpendicular to the ribbon plane (Fig. 2). A zone of columnar grains with the width of about 1 μm and length of about 10 μm was observed at the chilled surface of all materials. The width of this zone extends usually to the middle of the ribbon, however, at places with a smaller ribbon thickness (Fig. 3a) it may even disappear. A fine microcellular structure was observed in some columnar grains in the Al-Ti alloy (Fig. 3b). The zone adjoining the free surface exhibits a cellular structure with the mean size of individual equiaxed cells of about 1 μm in the Zr-rich alloys ($x > 0.5$) (Fig. 2). Numerous regions with the petal-like morphology were observed in Ti-rich alloys with $x \leq 0.25$ (Fig. 3b).

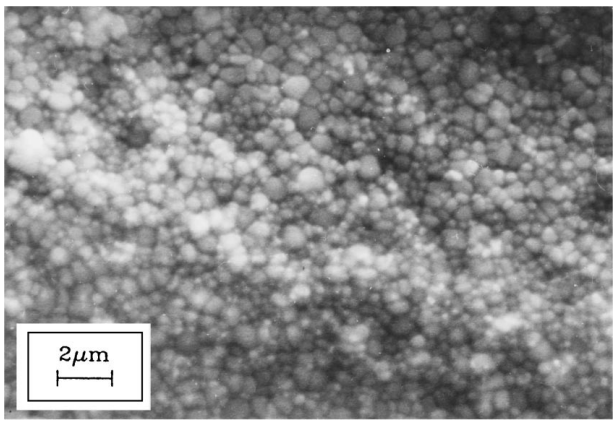

Figure 1 The structure of the free surface in the as melt-spun Al-Zr-Ti ribbon, $x = 0.75$, SEM.

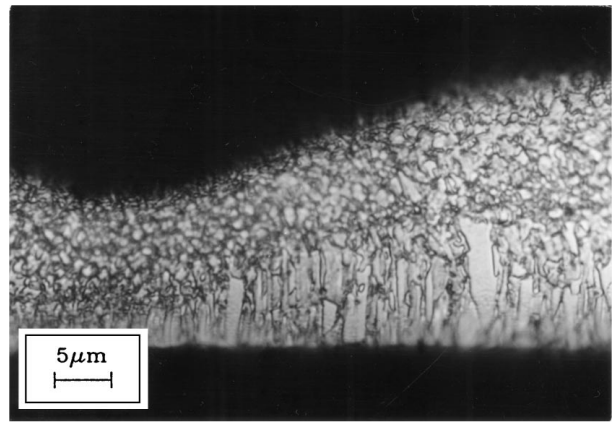

Figure 2 The grain structure of the Al-Zr-Ti alloy, $x = 0.5$, light microscopy.

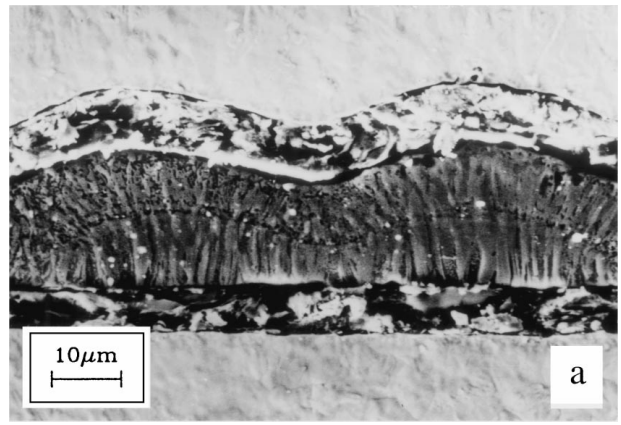

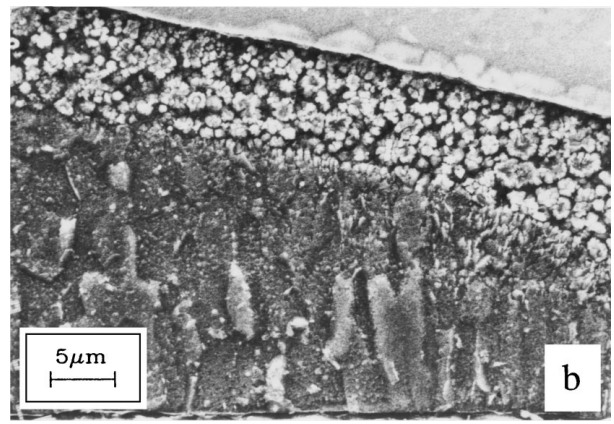

Figure 3 The grain structure of the Al-Zr-Ti alloys revealed on the longitudinal section of ribbons (SEM) (a) Al-Zr alloy, (b) Al-Ti alloy.

WDA point analyses were performed on transversal sections in series along lines going through the regions of a different ribbon thickness parallel to the ribbon plane. No statistically significant differences in the chemical composition were revealed. Further series of point analyses were performed along lines perpendicular to the ribbon plane in order to detect a possible gradient in the chemical composition. Most of measurements showed no compositional gradient within the experimental error of the measuring methods. In some cases a slightly higher content of Zr and Ti (about 0.2

TABLE II Knoop microhardness in the as melt-spun ribbons of the Al-$Al_3(Zr_xTi_{1-x})$

x	1	0.75	0.5	0.25	0
HK [kg/mm^2]	103 ± 22	112 ± 15	110 ± 25	62 ± 3	48 ± 6

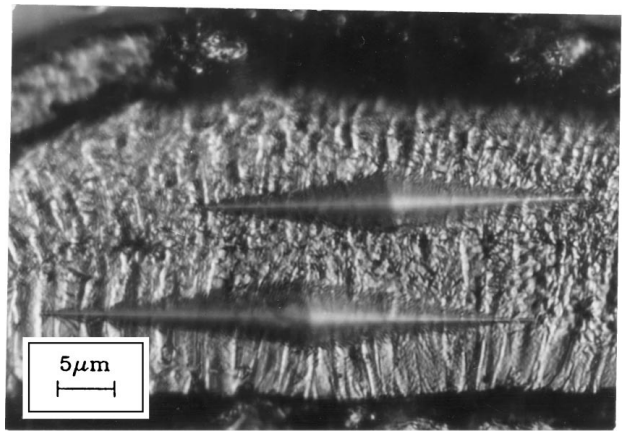

Figure 4 The influence of the solidification structure on Knoop microhardness, Al-Zr alloy (OM).

wt.%) was found near the free surface. The minimum effective area of the point analysis of several μm^2 did not allow to detect any second phase particles the sizes of which are expected to be much smaller or any solute microsegregations in microcell walls.

Mechanical properties were characterized by Knoop microhardness (HK). Table II presents the mean HK values measured in the as melt-spun ribbons. Each of these mean values represents an average from at least 20 measurements. It is obvious that the microhardness is much higher in the Zr-rich alloys ($x \geq 0.5$) than in the Ti-rich ones. The former alloys exhibit a much broader scatter in the HK values (e.g. values between HK = 70 and 154 were measured in the binary Al-Zr alloy). A detailed investigation was performed to identify the reasons of this scatter. It was found that statistically higher values of Knoop microhardness were measured at places with larger ribbon thickness. At thicker places the indents were applied at various distances from the chilled surface. The highest values were found in the middle of the ribbon, the lowest values close to the chilled surface. A correlation with the solidification structure revealed statistically lower values of microhardness in the zone of columnar grains (Fig. 4).

3.2. Phase composition

The SAXS curves measured in all materials are given in Fig. 5. The mean square fluctuation of the scattering density $\overline{(\Delta\rho)^2}$ was calculated from the integrated scattering density as [14]

$$\overline{(\Delta\rho)^2} = \frac{K}{4\pi^2}\int_0^\infty \frac{\mathrm{d}\Sigma}{\mathrm{d}\Omega}(q) q \, \mathrm{d}q \qquad (1)$$

where $\mathrm{d}\Sigma/\mathrm{d}\Omega$ is the normalized intensity measured with an infinitely long primary beam (smeared intensity), q is the scattering vector, and K is an instrument constant. This procedure may be applied only in Zr-rich

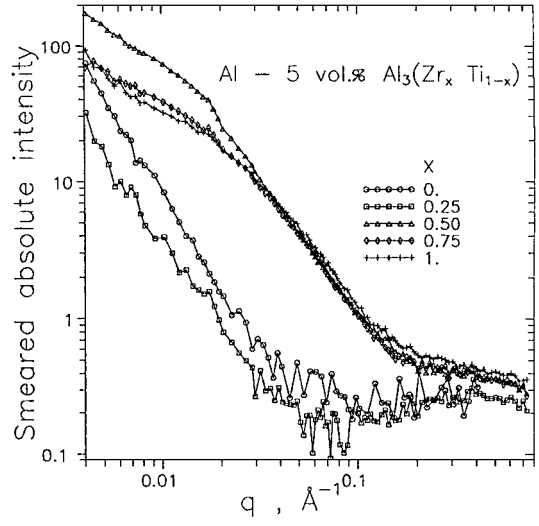

Figure 5 SAXS curves in the as melt-spun Al-Zr-Ti alloys.

alloys ($x \geq 0.5$) where the scattering curves can be extrapolated to zero scattering vectors with a reasonable accuracy. Nevertheless, even in these alloys the experimental error of $(\Delta\rho)^2$ is about 20%.

A two-phase model was adopted in order to deduce some quantitative structural data from SAXS curves. According to this model, the mean square fluctuation of scattering density can be then written as

$$\overline{(\Delta\rho)^2} = v_1 v_2 (\rho_1 - \rho_2)^2 \qquad (2)$$

where v_i and ρ_i are the volume fractions and scattering densities of the matrix and second phase particles, respectively. The $Al_3(Zr_xTi_{1-x})$ phase is considered as that forming the second phase particles. Table III shows the comparison of experimental values $\overline{(\Delta\rho)^2}_{\mathrm{exp}}$ with theoretical ones calculated on the assumption of the phase equilibrium characterized by negligible solid solubilities of Zr and Ti in Al-matrix and, therefore, by the presence of 5 vol.% of the $Al_3(Zr_xTi_{1-x})$ particles. A big difference between experimental and theoretical values of $\overline{(\Delta\rho)^2}$ shows that the alloys are far from equilibrium and the volume fraction v_2 of second phase particles is close to 2%.

Scattering behaviour at high scattering vectors can be described by a modified Porod's law [15]

$$\frac{\mathrm{d}\Sigma}{\mathrm{d}\Omega}(q) = A + \frac{C_3}{q^3} \qquad (3)$$

Assuming the simplest model of spherical second phase particles, their diameter D can be evaluated by the

TABLE III The results of SAXS measurements

x	$\overline{(\Delta\rho)^2}_{\mathrm{exp}} 10^{20}$ cm^{-4}	$\overline{(\Delta\rho)^2}_{\mathrm{th}} 10^{20}$ cm^{-4}	v_2 [%]	D [nm]
1	1.5	5.6	1.4	6
0.75	1.4	4.4	1.6	6
0.5	1.8	3.3	2.8	8
0.25	—	2.3	—	460
0	—	1.4	—	120

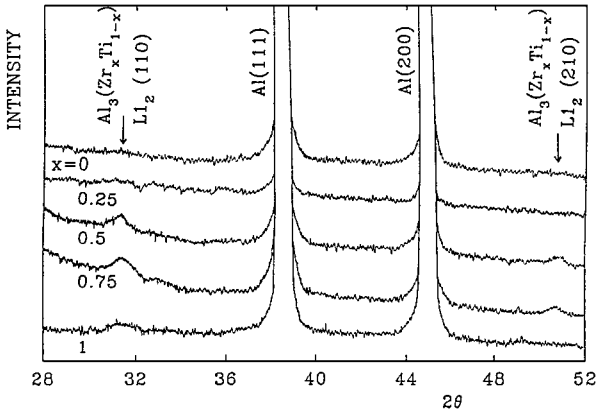

Figure 6 The X-ray diffractograms of the as melt-spun ribbons.

following equation

$$D = \frac{6v_2}{KC_3}\pi^2(\rho_1 - \rho_2)^2 \tag{4}$$

where

$$C_3 = \lim_{q\to\infty} q^3\left(\frac{\mathrm{d}\Sigma}{\mathrm{d}\Omega}(q) - A\right) \tag{5}$$

Table III shows that the characteristic size of second phase particles in Zr-rich alloys is several nanometers. The volume fraction of second phase particles in Ti-rich alloys is not known. The resulting characteristic size of second phase particles seems to be much bigger than in Zr-rich alloys even for a hypothetical value of $v_2 = 1\%$.

The X-ray diffraction analysis represents an alternative method for the investigation of the phase composition. Fig. 6 shows that beside the Al-based matrix peaks, only very small peaks corresponding to (110) and (210) reflections of the metastable $Al_3(Zr_xTi_{1-x})$ phase with the cubic $L1_2$ structure can be detected in the Zr-containing alloys. No extra peaks were found in the Al-Ti alloy. The measured lattice parameters, both of the matrix and second phase, are summarized in Table IV.

Table IV shows a nearly constant lattice parameter of the matrix in Zr-rich alloys. A slight decrease in the matrix lattice parameter exceeding the experimental error was found in Ti-rich alloys. The measured values are compared with the theoretical values computed for two hypothetical states:

a) all Zr and Ti atoms are dissolved in the supersaturated matrix

b) the amounts of Zr and Ti atoms dissolved in the matrix correspond to the equilibrium solid solubility limits

It was reported that Zr atoms extend the lattice parameter of Al by 0.00168 nm/at.% [16] and Ti atoms shrink it by −0.00105 nm/at.% [17]. The matrix lattice parameters corresponding to the case a) are marked as a_{ss} in Table IV. The equilibrium solid solubilities are about 0.01 wt.% Zr and 0.025 wt.% Ti at room temperature [4]. Such small amount of solutes cannot influence the lattice parameter of the Al-matrix and, therefore, the lattice parameter of pure Al can be used as the lattice parameter a_{eq} for the case b). It can be seen that the measured lattice parameters of the matrix do not simply correspond to any of both models.

The detection of non-matrix phases is very difficult in the alloys studied, especially because of their low volume fraction. In addition, the structure of expected $Al_3(Zr_xTi_{1-x})$ phases is similar to that of pure Al and their most intensive diffraction peaks are overlapped by matrix peaks. The presence of second phases may be then proved only by the detection of some less intensive diffraction extra peaks resulting from the ordering of these phases. The extra peaks observed in our as melt-spun ribbons are very small and diffuse. Their half-width is about 0.4° and the corresponding experimental error in the lattice parameter may be then estimated to about 0.001 nm. Table IV shows a good correlation of the measured parameters with the values determined by the interpolation from the known lattice parameters of both metastable Al_3Zr and Al_3Ti phases [2].

3.3. Internal structure

The above given results suggest significant differences between the Zr-rich ($x \geq 0.5$) and Ti-rich ($x \leq 0.25$) alloys. Moreover, TEM experiments confirmed differences also in the internal structure. Fig. 7a shows the typical structure of the Zr-rich alloys at low magnification. The mean grain size evaluated from micrographs is below 1 μm in all these alloys . The interfaces exhibit a marked curvature. A slightly coarser structure with the mean grain size of about 2 μm was found in Ti-rich alloys (Fig. 7b). The most interfaces are straight and meet at tripple points characterized by dihedral angles close to the equilibrium value of 120°.

TABLE IV Lattice parameters of phases present in the as melt-spun ribbons

	a (matrix) [nm]			a (Al_3(Zr, Ti)) [nm]	
		Computed			
x	Measured	a_{ss}	a_{eq}	Measured	Theoretical
1	0.4049 ± 0.0004	0.4071	0.4050	0.408 ± 0.001	0.4077
0.75	0.4049 ± 0.0004	0.4062	0.4050	0.405 ± 0.001	0.4050
0.5	0.4051 ± 0.0004	0.4054	0.4050	0.404 ± 0.001	0.4022
0.25	0.4045 ± 0.0004	0.4045	0.4050	0.399 ± 0.001	0.3994
0	0.4042 ± 0.0004	0.4036	0.4050	—	0.3967

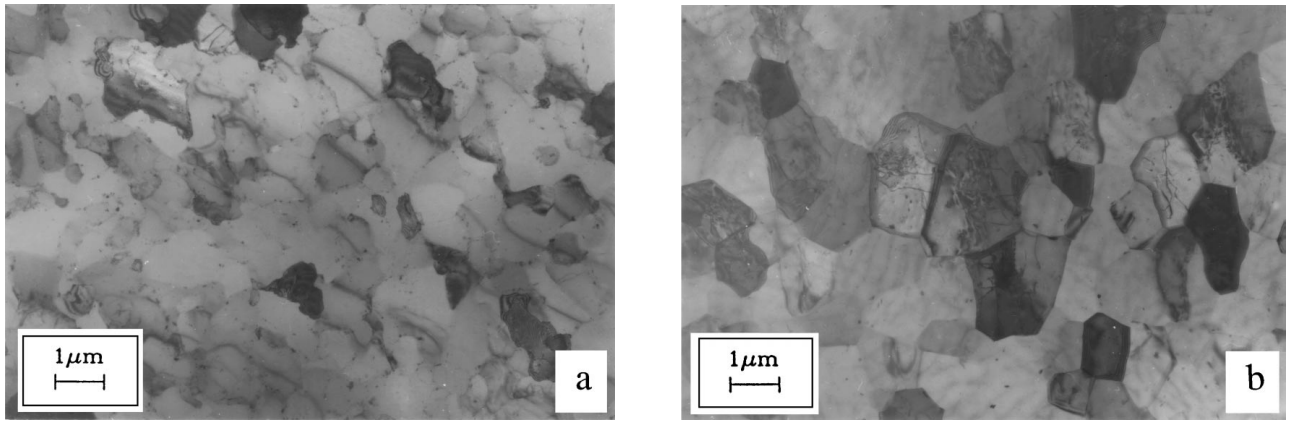

Figure 7 The internal structure of the as melt-spun ribbons (TEM): (a) $x = 0.5$, (b) $x = 0$.

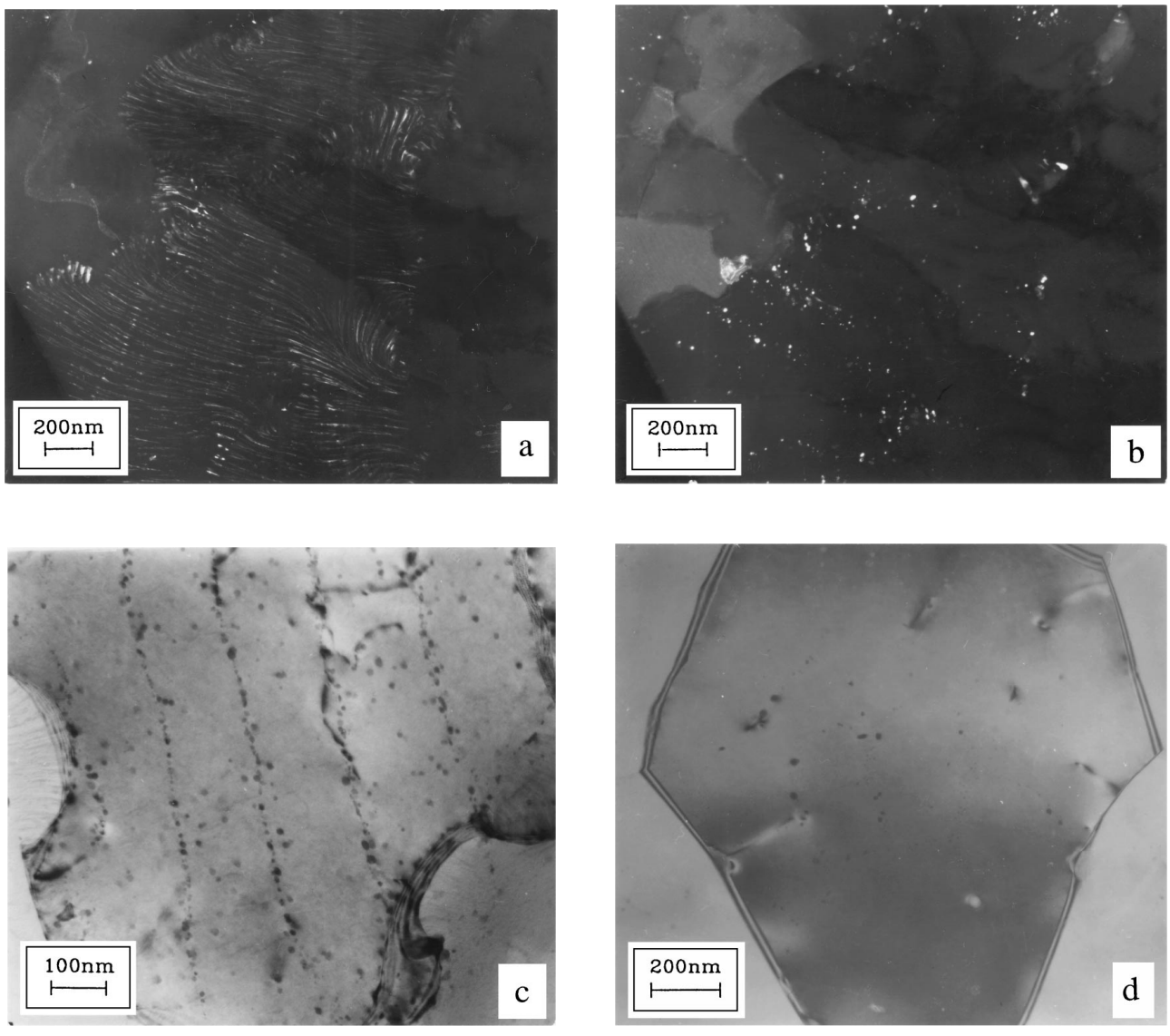

Figure 8 The particles present in the as melt-spun ribbons (TEM): (a) $x = 0.5$, dark field in (110) reflection of coherent $L1_2$ phase modification, (b) $x = 0.5$, the same place, dark field in (111) reflection of non-coherent $L1_2$ phase modification, (c) $x = 0.5$, (d) $x = 0$.

A typical feature of Zr-rich alloys is the presence of two types of particles—very fine particles (below 4 nm) arranged into a fan shaped morphology (Fig. 8a) and individual coarser (about 10 nm), probably spherical particles located both between the arms of fans and at boundaries (Fig. 8b). At some places (Fig. 8c), the individual particles are arranged into arrays. Electron diffraction experiments proved the fans to be formed by coherent particles of the metastable $Al_3(Zr_xTi_{1-x})$ phase with the cubic $L1_2$ structure in the "cube to cube" orientation relationship to the matrix. The individual particles are probably formed by the same phase,

however, they are not coherent with the matrix. The ratio of grains exhibiting the fan shaped precipitation decreases rapidly in the Al-Zr-Ti alloys with $x = 0.25$ and no fans were observed in the Al-Ti alloy (Fig. 8d). Only individual coarser particles were observed both within grains and at interfaces. The presence of Fe was proved in many of these particles.

4. Discussion

4.1. Solidification structure

The Al-based alloys containing Zr, V or Ti which were suggested as candidates for elevated temperature applications should deduce their high strength from a very dense distribution of small second phase particles formed due to a precipitation reaction in solid state. A microsegregation free solidification structure is a desirable precursor for this reaction. It was shown that such a solidification structure cannot be achieved using chill casting [18, 19]. Coarse petal-like particles composed of a dendritic structure of the $L1_2$ Al_3Zr or Al_3Ti phases and Al-based matrix were usually formed at the centers of grains [20, 21, 22]. A new way to a microsegregation free structure was open by the development of rapid solidification techniques. Especially the melt spinning method characterized by cooling rates of about 10^6 Ks^{-1} is often used in laboratory experiments.

The solidification structure of as melt-spun ribbons of Al-based alloys consists generally of two zones [23]. The zone A adjoining the chilled surface of the ribbon exhibits usually a featureless structure if observed in optical microscope. On the other hand, the zone B adjoining the free surface has typically a cellular or dendritic structure. A two zone solidification structure was observed in our Al-Zr-Ti alloys, too. The zone A was found to be formed by columnar grains which are decomposed to a microcellular structure in Ti-rich alloys. This result seems to be inconsistent with the above mentioned featureless structure. However, more detailed investigations performed with other Al-Zr based alloys revealed similar differences. Columnar grains were observed in Al-Zr-V alloys at places of a good contact of the melt with a wheel [16]. A cellular structure within grains was found both at binary Al-Zr alloys [24] and at Al-Zr-V alloys with a low V : Zr ratio [12]. Therefore, a fully microsegregation free solidification structure is not a general feature even at very high solidification rates.

The structure of the zone B was found cellular and dependent on the Zr : Ti ratio. An increasing amount of Ti favoures unambiguously a formation of petal like particles. This finding is in agreement with previous results on binary Al-Zr and Al-Ti alloys. In the Al-Zr alloys, the petal like particles were found only at low solidification rates of the order of 10 Ks^{-1} [20, 21] and no such particles were observed in rapidly solidified alloys even at very high Zr contents (up to 8.6 wt.%) [25]. On the other hand, the petal like particles in Al-Ti alloys were observed even in melt-spun specimens [22, 26, 27]. It was shown that solidification rates of 2×10^5 and 10^6 Ks^{-1} are necessary to suppress the formation of petal-like particles in Al-Ti alloys the composition of which is close to our Ti-rich Al-Zr-Ti alloys ($x \leq 0.25$) [22]. These values are in good agreement with solidification rates expected at the free surface of melt-spun ribbons.

4.2. Phase composition

Rapid solidification can extend the solid solubility of Zr and Ti in Al in a significant manner and suppress the formation of second phase particles. However, the data on the extented solid solubility limit and on the presence of second phase particles are very diverse. The explanation of this diversity can be sought not only in the composition of alloys and solidification rate in individual experiments but also in the selection of experimental methods used. TEM experiments give only a local information on the structure and, in case of inhomogeneous structures, the results may be misleading. The general information on the phase composition can be obtained using X-ray diffraction analysis. However, the volume fractions of second phases and the intensities of their diffraction peaks are very low. Also the changes in the lattice parameter of the Al-based matrix due to dissolved Zr and Ti lie usually within the experimental error. In order to avoid this difficulty and to get a more reliable information on the phase composition of the Al-Zr-Ti alloys studied, several experimental methods were combined.

SAXS measurements revealed unambiguously the presence of some centres contributing to the scattered intensity. Assuming that these centres are particles of the $Al_3(Zr_xTi_{1-x})$ phase their volume fractions and mean sizes were estimated. The volume fraction close to 2% in Zr-rich alloys represents only a very rough estimate. However, it can be concluded that the volume fraction of the second phase is deeply below the value corresponding to the phase equilibrium. Despite of many simplifications (a two phase model, the spherical form of particles) the SAXS results suggest clearly a different size of second phase particles in Zr-rich and Ti-rich alloys.

The experimental error of the lattice parameter of the matrix was estimated to be about ±0.0004 nm. This scatter excludes any reasonable conclusions on the phase composition of the Al-Zr-Ti alloys with $x = 0.25$ and 0.5. The decrease in the lattice parameter of the matrix in the Ti-rich alloys ($x \leq 0.25$) correlates with the expectation that rapid solidification extends the solid solubility of Ti in Al. However, the relatively low value of the matrix lattice parameter measured in the Al-Zr alloy is surprising as it suggests only a very low content of Zr atoms dissolved in the Al-matrix. Such an interpretation is incosistent both with SAXS results and with literature data. This discrepancy may be caused by the uncertainty of data relating to the influence of Zr on the lattice parameter of Al taken from [16]. Other experiments [25, 28] show also much weaker extension of the Al lattice due to dissolution of Zr - about 0.0004 nm/at.%. Considering this value and the volume fraction $v = 2\%$ resulting from SAXS experiments, the expected lattice parameter of the supersaturated Al-matrix in the Al-Zr alloy should be about 0.4052 nm which is very close to the value found experimentally.

The X-ray diffraction and TEM experiments enabled to identify the particle forming phase. Extra diffraction peaks observed in the Zr-rich Al-Zr-Ti alloys can be interpreted as (110) and (210) reflections of the metastable Al_3(Zr, Ti) phase with the $L1_2$ structure. The decrease in the lattice parameter of this phase with increasing Ti-content (see Table IV) supports the idea that Ti atoms substitute for Zr atoms in the Al_3Zr phase. The measured values of the lattice parameter agree well with the values calculated using the Vegard's law from lattice parameters of both Al-Zr and Al-Ti binary alloys. This suggests that the composition of the $Al_3(Zr_xTi_{1-x})$ corresponds well with the nominal composition.

The $Al_3(Zr_xTi_{1-x})$ phase appears mostly in the form of fans composed of very small particles in the Zr-rich ($x \geq 0.5$) alloys. A similar structure was reported in as melt-spun ribbons of the Al-3.3 wt.% Zr [29] and Al-5 vol.% $Al_3(Zr_{0.75}V_{0.25})$ [16] alloys. The fan shaped morphology is a typical feature in Al-Zr alloys aged at temperatures between 573 and 773 K [10, 24, 25, 29, 30]. *In-situ* TEM experiments confirmed that this structure was formed by a discontinuous reaction [31]. The same mechanism seems to be operating also in our Zr-rich alloys. Fig. 8c shows the grain boundary bulges which extend alternatively into opposite grains, create undulations of the boundary and contribute to a significant curvature of boundaries. A proper investigation of the structure within boundary bulges revealed that all of them contained very fine particles arranged into fans.

The formation of fans is very limited in the alloy with $x = 0.25$ and fully suppressed in the binary Al-Ti alloy. The absence of discontinuous reaction results into straight grain boundaries. A similar absence of fans was observed in the V-rich Al-Zr-V alloys [12, 16] where only individual spherical particles were observed. A very low lattice mismatch between the Al_3(Zr,V) particles and Al-matrix in these V-rich alloys was believed to reduce the energy barrier for homogeneous nucleation of particles and to support the formation of individual particles rather than discontinuously formed fans. This explanation does not seem plausible with our experiments in Al-Zr-Ti alloys. The lowest lattice mismatch should be achieved in the Al-Zr-Ti alloy with $x = 0.75$, i.e. in the alloy where the fans are very frequent. On the other hand, the Ti-rich alloys which do not exhibit fan shaped structure have much worse lattice mismatch. We suppose that the difference between the structure of Zr-rich Al-Zr-Ti alloys and Ti-rich Al-Zr-Ti alloys (and probably also V-rich Al-Zr- V alloys) is caused by substantially lower diffusion rate of Zr in Al as compared to that of V and Ti [32]. In the case of Zr, a much faster kinetic of diffusion along grain boundaries favoures the discontinuous reaction. A pining effect of particles located at grain boundaries in Ti-rich and V-rich [11, 12] Al-alloys may further suppress the migration of grain boundaries and, consequently, the discontinuous reaction.

The fans forming particles were found to be fully coherent with the Al-matrix. On the other hand, the individual particles seem to be only semicoherent. There may be two reasons for this orientation difference. Chen *et al*. [16] argued that the individual particles were originally formed in a coherent orientation which was distorted by the migration of the grain boundary during the discontinuous reaction. Another possibility is the preferential nucleation of these particles on dislocations, especially in case of individual particles arranged into arrays (see Fig. 8c). Similar bands within grains were observed in the structure of the rapidly solidified Al-6 wt.% Zr alloy [24] and interpreted as arrays of dislocations. This observation may support the latter explanation.

4.3. Microhardness

The difference between the microhardness values of the as melt-spun Zr-rich ($x \geq 0.5$) and Ti-rich ($x \leq 0.25$) Al-Zr-Ti alloys, respectively, exceeds 100%. As the grain size and solute content are nearly identical in both groups of alloys, the phase composition plays probably the decisive role in the explanation of the microhardness values. The HK values measured in the Ti-rich alloys are close to the value of HV = 59 found in the as melt-spun Al-3.9% Zr [25] and Al-0.54% Zr-2.23% V [33] alloys which have similar solute content as our alloys. Similarly to our Ti-rich alloys, the above mentioned alloys were found as nearly single-phase supersaturated solid solutions without the fan shaped arrangement of second phase particles. The main contribution to microhardness is probably given by solid solution strengthening in these materials.

The microhardness values measured in our as melt-spun Zr-rich alloys are closer to values reported for alloys of similar composition after ageing. The peak microhardness values of HV = 100 [33] and 140 [25] were obtained in ribbons of Al-Zr alloys which should contain about 2.5 and 4.8 vol.% of the Al_3Zr phase in a fully decomposed state, respectively. In both these materials the fan shaped precipitation was developed and it can be concluded that the precipitation strengthening due to the metastable coherent Al_3Zr particles is responsible for their high microhardness. Similar explanation seems to be valid in our Zr-rich alloys, too. The comparison of our HK values with the literature data [25] enables to estimate roughly the volume fraction of the $Al_3(Zr_xTi_{1-x})$ in our Zr-rich alloys as about 2%. This estimate agrees very well with the volume fraction resulting from SAXS experiments.

A remarkable scatter of microhardness values was observed in the Zr-rich Al-Zr-Ti alloys with a tendency to lower values in thinner parts of ribbons and in the zone adjoining the chilled surface. The WDA analysis proved the nonexistence of significant composition gradients through the ribbons. The variations in HK reflect probably a difference in the phase composition, i.e. a different degree of decomposition at various places of ribbons. As the rates of solidification and subsequent cooling decrease with increasing distance from the chilled surface a higher degree of decomposition is more probable in thicker parts of ribbons and in the zone adjoining the free surface. Therefore, higher values of microhardness can be expected at these places.

5. Conclusions

1. The solidification structure, the phase composition and the microhardness depend on the Zr : Ti ratio in the as melt-spun Al-Zr-Ti alloys. No composition gradients were observed in the ribbons.

2. The as melt-spun Ti-rich alloys ($x \leq 0.25$) are nearly single-phase. The few particles found in had the sizes up to 100 nm and contained frequently Fe.

3. The as melt-spun Zr-rich alloys ($x \geq 0.5$) contain second phase particles of the size below 10 nm which are preferentially arranged into fans. These particles are fully coherent with Al-matrix and were identified as the metastable $A1_3(Zr_xTi_{1-x})$ phase with the cubic Ll_2 structure. The contents of Zr and Ti in these particles are in good agreement with nominal compositions. The volume fraction of this phase reaches about 2%.

4. The microhardness values in the range between HK = 48 and 62 were found in Ti-rich alloys. The main contribution is expected from solid solution strengthening.

5. The microhardness values exceeding HK = 100 were found in Zr-rich alloys. The main contribution is expected from precipitation strengthening. The higher microhardness observed in the zone adjoining the free surface reflects a higher degree of decomposition at this place of ribbons.

Acknowledgements

The authors are grateful to Dr. D. Plischke, Crystal Laboratory Göttingen, Germany, for the preparation of thin ribbons. The research was supported by the Grant Agency of Charles University through the grant No. 283 and by the Grant Agency of Czech Republic through the grant No. 93-2432. Alexander von Humboldt Foundation has kindly donated the microhardness tester to the Department of Metal Physics of Charles University Prague.

References

1. H. JONES, *Aluminium* **54** (1978) 274.
2. S. SRINIVASAN, P. B. DESCH and R. B. SCHWARTZ, *Scripta Metall.* **25** (1991) 2513.
3. E. NES, *Acta Metall.* **20** (1972) 499.
4. L. F. MONDOLFO, "Aluminium Alloys: Structure and Properties" (Butterworth, London, 1976).
5. S. K. DAS and L. A. DAVIS, *Mater. Sci. Eng.* **98** (1988) 1.
6. H. JONES, "Rapid Solidification of Metals and Alloys" (Inst. of Metallurgists, London, 1982).
7. I. M. LIFSHITZ and V. V. SLYOZOV, *J. Phys. Chem. Solids* **19** (1961) 35.
8. C. WAGNER, *Z. Elektrochem.* **65** (1961) 581.
9. M. ZEDALIS and M. E. FINE, *Scripta Metall.* **17** (1983) 1247.
10. *Idem., Met. Trans. A* **17** (1986) 2187.
11. Y. C. CHEN, M. E. FINE, J. R. WEERTMAN and R. E. LEWIS, *Scripta Metall.* **21** (1987) 1003.
12. R. E. LEWIS, D. D. CROOKS, Y. C. CHEN, M. E. FINE and J. R. WEERTMAN, in Proceedings of the 3rd International Conference on Creep and Fracture of Engineering Materials, Swansea, 1987, edited by B. Wilshire and R. W. Evans (The Inst. of Metals, London, 1987) p. 331.
13. V. R. PARAMESWARAN, J. R. WEERTMAN and M. E. FINE, *Scripta Metall.* **23** (1989) 147.
14. O. KRATKY, *Prog. Biophys.* **13** (1963) 105.
15. W. RULAND, *J. Appl. Cryst.* **4** (1971) 70.
16. Y. C. CHEN, M. E. FINE and J. R. WEERTMAN, *Acta Metall. Mater.* **38** (1990) 771.
17. J. E. HETCH (ed.), "Aluminum: Properties and Physical metallurgy" (Metals Park, OH, ASM, 1974) p. 29.
18. T. OHASHI and R. ICHIKAWA, *Met. Trans.* **3** (1972) 2300.
19. E. NES and H. BILLDAL, *Acta Metall.* **25** (1977) 1039.
20. T. OHASHI and R. ICHIKAWA, *Z. Metallkde* **61** (1973) 517.
21. E. NES, H. BILLDAL, *Acta Metall.* **25** (1977) 1031.
22. S. HORI, H. TAI and Y. NARITA, in "Rapidly Quenched Metals," edited by S. Steeb and H. Warlimont (Elsevier Sci. Publ., 1985) p. 911.
23. H. JONES, *Mater. Sci. Eng.* **5** (1969/70) 1.
24. S. K. PANDEY, D. K. GANGOPADHYAY and C. SURYANARAYANA, *Z. Metallkde* **77** (1986) 12.
25. E. SAHIN and H. JONES, in "Rapidly Quenched Metals II, edited by B. Cantor (The Metals Soc., London, 1978) p. 138.
26. A. MAJUMDAR and B. C. MUDDLE, *Mater. Sci. Eng. A* **169** (1993) 135.
27. M. G. CHU, *ibid. A* **179/180** (1994) 669.
28. L. M. BUROV and A. A. YAKUNIN, *Russ. J. Phys. Chem.* **42** (1968) 540.
29. H. OCTOR and S. NAKA, *Phil. Mag. Letters* **59** (1989) 229.
30. N. RYUM, *Acta Metall.* **20** (1969) 499.
31. Z. A. CHAUDHURY and C. SURYANARAYANA, *Metallography* **17** (1984) 231.
32. H. M. LEE, *Scripta Metall. Mater.* **24** (1990) 2443.
33. W.-W. PARK and T.-H. KIM, *Scripta Metall.* **22** (1988) 1709.

Received 24 June 1996
and accepted 22 November 1999